The effect of water and fO_2 on the ferric–ferrous ratio of silicic melts

Fabrice Gaillard [*], Bruno Scaillet, Michel Pichavant, Jean-Michel Bény

CRSCM-CNRS, 1A rue de la Férollerie, Orleans Cedex 02 45071, France

Abstract

New experiments on the effect of dissolved water on the ferric–ferrous ratio of silicic melts have been performed at 200 MPa, between 800°C and 1000°C and for fO_2 between NNO − 1.35 and NNO + 6.6. Water-saturated conditions were investigated. Compositions studied include six metaluminous synthetic melts, with FeO_{tot} progressively increasing from 0.47 to 4.25 wt.%, two natural obsidian glasses (one peraluminous and the other peralkaline) and a synthetic rhyolitic glass having the composition of the matrix glass of the June 15, 1991 Pinatubo dacite. Ferrous iron was analyzed by titration and FeO_{tot} by electron microprobe. Variation of quench rate was found to have no detectable effect on the ferric–ferrous ratio of the hydrous silicic melts investigated. At NNO, no dependence of the ferric–ferrous ratio with temperature is observed. At $fO_2 <$ NNO + 1, metaluminous melts have ferric–ferrous ratios higher than calculated from the Kress and Carmichael (KC) (Kress, V.C., Carmichael, I.S.E., 1991. The compressibility of silicate liquids containing Fe_2O_3 and the effect of composition: temperature: oxygen fugacity and pressure on their redox states. Contrib. Mineral. Petrol. 108, 82–92.) empirical equation (i.e., water has an oxidizing effect relative to KC), whereas at $fO_2 >$ NNO + 1, the experimental ferric–ferrous ratios are equal or lower than calculated. The peralkaline samples show the same type of behaviour. A non-linear relationship between $X_{Fe_2O_3}/X_{FeO}$ and fO_2 implies that a term for dissolved water must be added to the KC equation if it is to be applied to the calculation of ferric–ferrous ratios of hydrous silicic melts. Above NNO + 1, the ferric–ferrous ratio is essentially controlled by the anhydrous melt composition and fO_2. However, differences exist between measured and calculated ferric–ferrous ratios of silicic melts that are not all attributable to the effect of dissolved water. Additional work is needed to describe more precisely the dependence of the ferric–ferrous ratio on anhydrous melt composition. The oxidizing effect of water is restricted to relatively reduced magmatic liquids. In oxidized calk-alkaline magma series, the presence of dissolved water will not largely influence melt ferric–ferrous ratios. © 2001 Elsevier Science B.V. All rights reserved.

*Keywords:* Iron; Water; Oxygen fugacity; Silicic melts

1. Introduction

Knowledge of the oxidation state of iron in silicate melts is a key for understanding the physical and the chemical evolution of magmas during differentiation (Osborn, 1959; Carmichael and Ghiorso, 1990). The ferric–ferrous ratio plays an important role on melts properties such as density or viscosity (Lange and Carmichael, 1990; Dingwell, 1991; Dingwell and Brearley, 1988). It also controls the

[*] Corresponding author.

appearance of iron-bearing oxides and ferromagnesian silicates, and the chemical composition of the coexisting melt. From a general point of view, the ferric–ferrous ratio of silicate melts is related to oxygen fugacity (fO_2) by the following equilibrium:

$$\underset{\text{melt}}{2FeO} + \underset{\text{gas}}{1/2\,O_2} \Leftrightarrow \underset{\text{melt}}{Fe_2O_3}, \tag{1}$$
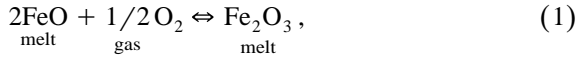
$$K = a_{Fe_2O_3}/(a_{FeO})^2(fO_2)^{1/2}. \tag{2}$$

Therefore, knowledge of the ferric–ferrous ratio of a given silicate melt should enable fO_2 to be calculated. However, several authors have pointed out that, in addition to fO_2, the ferric–ferrous ratio is dependent on the composition of the melt (e.g., Sack et al., 1980; Thornber et al., 1980; Dickenson and Hess, 1981). Empirical relations have been proposed to describe the effects of melt composition, fO_2, temperature and pressure on the ferric–ferrous ratio of silicate melts (e.g., Sack et al., 1980; Kilinc et al., 1983; Mysen, 1988; Borisov and Shapkin, 1990; Kress and Carmichael, 1991; hereafter designated as KC). These equations have the following general form (Sack et al., 1980; Kilinc et al., 1983; KC):

$$\ln\left(X_{Fe_2O_3}/X_{FeO}\right) = a\ln fO_2 + b/T + c$$
$$+ \Sigma d_i X_i + f(T,P), \tag{3}$$

where a, b, c are empirical constants, and X_i is the mole fraction of K_2O, Na_2O, Al_2O_3, FeO, CaO in the melt (KC). The $\Sigma d_i X_i$ term expresses the compositional dependence of the ferric–ferrous ratio. For instance, it is well known that, for a given fO_2, peraluminous melts display lower Fe^{3+}/Fe^{2+} ratios than their peralkaline equivalents (Douglas et al., 1965; Dickenson and Hess, 1981, 1986). However, the compositional dependence of the ferric–ferrous ratio is presently established on the basis of experimental data for dry melts. Water is a major component of most natural magmas, with concentrations commonly exceeding 1 wt.% and reaching, in some cases, 7 wt.% (see Johnson et al. 1994), which corresponds to a mole fraction of up to ~ 0.2 for a rhyolitic melt. Water strongly affects the physical and chemical properties of silicate melts and it might be anticipated that water also has an effect on melt Fe^{3+}/Fe^{2+} ratios. Carmichael (1991) found systematic differences between fO_2 calculated from Eq. (3) and from Fe–Ti oxides for several intermediate to silicic glassy lavas, and discussed the possibility that water dissolved in the lavas influences the ferric–ferrous calibration.

To date, only two experimental studies have investigated the effect of water on the oxidation state of iron in silicate melts (Moore et al., 1995; Baker and Rutherford, 1996). Moore et al. (1995) have carried out experiments under both H_2O-saturated and dry conditions on three natural compositions (a minette, an andesite and a peralkaline rhyolite). A total of 22 H_2O-saturated experiments were performed in the pressure range 50–200 MPa, between 950°C and 1130°C, and under oxidizing conditions (about 1–2log units above the Ni–NiO solid buffer, i.e., NNO + 1–2). Dissolved water has no significant effect on the ferric–ferrous ratio under the experimental conditions investigated by Moore et al. (1995). Baker and Rutherford (1996) presented data from 43 hydrous experiments, performed between 10 and 200 MPa (mostly at 200 MPa), 725°C and 1140°C and at fO_2 ranging from NNO up to MNO (i.e., the MnO–Mn_3O_4 solid buffer, equivalent to about NNO + 2.5). Two rhyolitic compositions, one metaluminous and the other peralkaline, were investigated. In contrast to Moore et al. (1995), Baker and Rutherford (1996) observed that the addition of water increases the Fe^{3+}/Fe^{2+} ratio of silicate melts in certain regions of the P–T–fO_2 space. For metaluminous melts, this oxidizing effect of water is well marked at NNO and for temperatures above 900°C, whereas at NNO + 2.5 or at low temperatures, water has no effect. For peralkaline melts, an oxidizing effect of water was found both at NNO and NNO + 2.5 (Baker and Rutherford, 1996), in contrast with the results of Moore et al. (1995) for similar melt compositions. It is worth emphasizing that the effect of water on the ferric–ferrous ratio has been determined to date for a narrow range of fO_2, near the oxidizing end of the spectrum of redox conditions for natural magmas (NNO to NNO + 2.5; Moore et al., 1995; Baker and Rutherford, 1996), and that it remains unknown for moderately to strongly reducing conditions ($fO_2 < $ NNO). Important classes of melt compositions, such as peraluminous compositions, are presently excluded from the available database for hydrous melts.

In this study, we report new experimental determinations of the ferric–ferrous ratio of hydrous (H_2O-saturated) silicic melts at 800°C, 930°C and 1000°C, and 200 MPa. In contrast to previous studies (Moore et al., 1995; Baker and Rutherford, 1996), a wide range of fO_2 conditions was investigated (from NNO − 1.35 to NNO + 6.6). Both synthetic and natural melt compositions have been studied. The data enable the effects of iron concentration and A/CNK see Table 1 on the ferric–ferrous ratio of hydrous silicic liquids to be evaluated.

2. Starting products

Nine rhyolitic melt compositions were investigated (Table 1). A series of six metaluminous synthetic melt compositions in the system Si–Al–Na–K–H–Fe–O was prepared by adding increasing amounts of iron (from 0.47 to 4.25 FeO_{tot}, Table 1) to the composition of the 200 MPa H_2O-saturated minimum of the haplogranite system (Holtz et al., 1992). The other three compositions studied are: a peraluminous obsidian glass from Macusani, Peru (Pichavant et al., 1987), a peralkaline obsidian from Ascension island (Harris, 1983), and a synthetic rhyolitic glass having the composition of the matrix glass of the June 15, 1991 Pinatubo dacite (Scaillet and Evans, 1999).

All synthetic compositions were prepared using a standard gel method (e.g., Pichavant, 1987). The fired gels were melted at 1400°C, 1 bar in air ($fO_2 = 0.2$ bar). The resulting glasses, as well as the two natural obsidians, were then ground in an agate mortar down to a mesh size of 20 μm. These glass powders were used as starting products in all the experiments. The capsules consisted of 150–200 mg of powdered starting material plus roughly 8 wt.% of distilled and demineralized H_2O loaded in Au tubes (25 mm length, ID: 5 mm, OD: 5.4 mm), which were arc-welded. The capsules were weighted before and after the experiments to check for leaks.

3. Experimental methods

Two internally heated pressure vessels (IHPVs) operating vertically were used in all experiments at 930°C and 1000°C. Temperature was controlled by means of two to three sheathed Ni–Cr thermocouples calibrated against the melting point of NaCl at 1 bar. The hot spot zone is 4–6 cm long and the temperature variation across the capsules never exceeded 2°C. Temperature fluctuation during the run was within 1°C of the setpoint. Overall, the maximum error on temperature is ±5°C. The vessels were pressurized either with pure Ar or with Ar–H_2 mixtures, depending on the desired redox conditions (see Scaillet et al., 1995 for additional details). Total pressure was monitored with transducers calibrated against an Heise Bourdon tube gauge and is known to within 2 MPa. Redox conditions were imposed

Table 1
Electron microprobe compositions of starting glasses

	No. 1	No. 2	No. 3	No. 4	No. 5	No. 6	Macusani	Pinatubo	Ascension
SiO_2	79.18	78.33	77.17	77.08	76.77	76.2	74.27	78.44	73.57
Al_2O_3	11.82	11.77	12.07	11.79	11.45	11.50	16.27	12.59	12.32
FeO[a]	0.47	0.83	1.71	2.58	3.38	4.25	0.59	1.00	3.17
MgO	0	0	0	0	0	0	0.01	0.21	0
CaO	0	0	0	0	0	0	0.2	1.33	0.32
Na_2O	3.83	4.05	4.02	3.74	3.71	3.67	4.32	3.31	5.54
K_2O	4.68	4.97	4.72	4.76	4.67	4.36	3.70	2.89	4.68
TiO_2	0	0	0	0	0	0	0.02	0.17	0.24
P_2O_5	0	0	0	0	0	0	0.53	0.02	0.03
Total[b]	99.98	99.90	99.85	99.90	99.98	100.06	98.35	99.89	99.91
A/CNK[c]	1.04	0.98	1.06	1.04	1.03	1.07	1.37	0.94	0.80

[a] Total iron expressed as FeO.
[b] All compositions recalculated on a H_2O- (and F-, B-, Li-) free basis; original total is reported.
[c] A/CNK = $Al_2O_3/(Na_2O + K_2O + CaO)$, in moles.

and controlled by the fH_2 prevailing in the pressure vessel. For fO_2 below NNO + 2 (runs 2–4, Table 2), different Ar/H_2 ratios were used to generate different fH_2 values, which were continuously monitored using a modified semi-permeable H_2 membrane (Scaillet et al., 1992) connected to a small

pressure transducer calibrated against a Protais tube gauge. The uncertainty in H_2 pressure reading is about 0.001 MPa for $fH_2 = 0.1$ MPa, and 0.01 MPa for $fH_2 = 5$ MPa. For fO_2 higher than NNO + 2 (run 1, Table 2), experiments used pure Ar as the pressurizing medium, and the redox conditions were

Table 2
Experimental conditions, run products and phase proportions

Charge number	Starting composition number	Run products[a]	Proportion of crystalline phases (wt.%)	ΔFeO_{tot}^b %
Run 1, P = 228 MPa, T = 923°C, fH_2^c = 0.001 MPa, ΔNNO^d = +6.6, duration = 84 h				
1/1	1	gl, fl	–	+15
1/2	2	gl, fl	–	−4
1/3	3	gl, fl, hm	0.6	–
1/4	6	gl, fl, hm	3.5	–
1/7	Ascension	gl, fl, hm	0.3	–
1/8	Pinatubo	gl, fl	–	−9
1/9	Macusani	gl, fl	–	+5
Run 2, P = 216 MPa, T = 926°C, fH_2 = 0.19 MPa, ΔNNO = 1.55, duration = 120 h				
2/1	1	gl, fl	–	+11
2/2	2	gl, fl	–	+5
2/3	3	gl, fl	–	0
2/4	4	gl, fl, mag	0.9	–
2/5	5	gl, fl, mag	1.7	–
2/6	6	gl, fl, mag	2.6	–
2/7	Ascension	gl, fl	–	+3
2/8	Pinatubo	gl, fl	–	−4
Run 3, P = 213 MPa, T = 927°C, fH_2 = 2.5 MPa, ΔNNO = −0.72, duration = 110 h				
3/1	1	gl, fl	–	+4
3/2	2	gl, fl	–	+2
3/3	3	gl, fl	–	+1
3/4	4	gl, fl	–	0
3/5	5	gl, fl, fay	1.1	–
3/6	6	gl, fl, fay	1.9	–
3/7	Ascension	gl, fl	–	+1
3/8	Pinatubo	gl, fl	–	−3
3/9	Macusani	gl, fl	–	−3
Run 4, P = 201 MPa, T = 927°C, fH_2 = 5.2 MPa, ΔNNO = −1.35, duration = 110 h				
4/1	1	gl, fl	–	−23
4/2	2	gl, fl	–	−37
4/3	3	gl, fl	–	−48
4/4	4	gl, fl	–	−35
4/5	5	gl, fl	–	−40
4/6	6	gl, fl	–	−37
4/7	Ascension	gl, fl	–	−10
4/8	Pinatubo	gl, fl	–	−46
4/9	Macusani	gl, fl	–	−27

[a] gl: glass; fl: fluid; hm: haematite; mag: magnetite; fay: fayalite.

[b] $\Delta FeO_{tot} = 100(FeO_{tot}$ glass $- FeO_{tot}$ starting composition$)/FeO_{tot}$ starting composition.

[c] fH_2 value from NiPdO sensor. All other fH_2 values are from the semi-permeable H_2 membrane.

[d] $\Delta NNO = \log fO_2$(experiment) $- \log fO_2$(NNO, at P and T).

fixed by the intrinsic $f\mathrm{H}_2$ of the pressure vessels. In all but one experiment (run 3, Table 2), $f\mathrm{H}_2$ was also measured with either Ni–Pd–O or Co–Pd–O solid sensors following the procedures of Taylor et al. (1992). The sensor material consisted of either Ni–Pd–NiO ($f\mathrm{O}_2 >$ NNO) or Co–Pd–CoO ($f\mathrm{O}_2 >$ Co–CoO or CCO buffer) powdered mixtures loaded with distilled and deionized water in Pt capsules (length: 25 mm, ID: 2.5 mm; OD: 2.9 mm) lined with ZrO_2 powder. After the experiments, the composition of the metallic alloy was determined by electron microprobe, then the $f\mathrm{O}_2$ was calculated from the empirical regression of Pownceby and O'Neill (1994) and finally, the $f\mathrm{H}_2$ computed from the water dissociation equilibrium (see below). The $f\mathrm{H}_2$ measured with the H_2 membrane agreed to within less than 1% with that given by the sensor, in agreement with previous work (Scaillet and Evans, 1999). Experiments were ended by switching off the power supply which resulted in quench rates of about 1–3°C/s for the first 300°C. In these experiments, quenching was not isobaric and pressure dropped by about 30 MPa during the first 300°C.

In order to test for potential quench effects on melt $\mathrm{Fe}^{3+}/\mathrm{Fe}^{2+}$ ratios, we performed a number of test experiments both at 1000°C and 800°C. At 1000°C, the IHPV was fitted with a drop quench device modified after Roux and Lefèvre (1992) (see also Holloway et al., 1992), allowing quench rates of the order of 300°C/s. We used two compositions: Ascension and the synthetic metaluminous composition with 1.71 wt.% FeO_{tot} (no. 3, Table 1). Because of the limited room available in the pressure vessel when fitted with the rapid-quench device, $f\mathrm{H}_2$ and $f\mathrm{O}_2$ were determined from the sensor technique (Co–Pd–O) only. Four capsules (two for each composition) were run together at 1000°C, 200 MPa for 4 days, then quenched under different rates. Two capsules (one for each composition) were drop-quenched by switching on the power supply on the hanging Pt wire (see Roux and Lefèvre, 1992), while the two other capsules remained attached in the hot spot zone and were quenched under normal rates. This procedure ensures that any difference in $\mathrm{Fe}^{3+}/\mathrm{Fe}^{2+}$ ratios can be interpreted unambiguously as due to different quench rates. At 800°C, externally heated hydrothermal pressure vessels (e.g., Pichavant, 1987) were used. Different quench rates were

imposed by performing either a drop quench of the capsule (rapid quench) or by leaving the vessel to cool in air (slow quench). In these experiments, redox conditions were controlled by the double capsule oxygen buffer technique, with either NNO or CCO buffer assemblages. Two compositions (Ascension and Pinatubo, Table 1) were tested.

All experiments were performed with a small amount of excess water and are considered water-saturated. Although the proportion of H_2 present in the fluid phase increases along with decreasing $f\mathrm{O}_2$ and reaches values up to the mole percent level in the most reduced experiments (e.g., 1.2 mol% in run 4, Table 2), a pure water fluid phase has been assumed. Therefore, $f\mathrm{H}_2\mathrm{O}$ equals the fugacity of pure water at P and T. Oxygen fugacity is calculated from the water dissociation equilibrium:

$$f\mathrm{O}_2 = \left(K_\mathrm{w} f\mathrm{H}_2\mathrm{O}/f\mathrm{H}_2 \right)^2, \qquad (4)$$

where $f\mathrm{H}_2\mathrm{O}$ is taken from Burnham et al. (1969), $f\mathrm{H}_2$ is experimentally measured (with membrane or sensor, see above), and K_w is taken from Robie et al. (1978).

Most experiments were carried out at 930°C. A few others were performed at 800°C and 1000°C (tests of the effect of quench rate on ferric–ferrous ratios). Pressure was kept constant at 210 ± 2 MPa. The choice of 930°C as the main experimental temperature was guided by several practical reasons. First, it allows to use Au capsules as containers and thus reduces the iron loss problem. Second, it is a temperature high enough to prevent crystallisation of water-saturated rhyolitic melts. Third, 930°C is within the temperature range examined by Baker and Rutherford (1996) and only slightly lower than that of Moore et al. (1995), which facilitates comparison between the different studies. Finally, this is a temperature meaningful for silicic magmas (e.g., Martel et al. 1998), which ensures that our results are applicable to natural conditions without requiring extrapolation far outside the calibrated range. Run durations varied between 4 and 6 days, similar to previous studies (Baker and Rutherford, 1996). At 930°C, four $f\mathrm{O}_2$ values were investigated: NNO + 6.6, NNO + 1.55, NNO − 0.72, NNO − 1.35, at 800°C, two $f\mathrm{O}_2$ values: NNO, NNO − 1.6 and at 1000°C, one $f\mathrm{O}_2$ value: ∼ NNO. Reversals have not

been performed in this study (but see Baker and Rutherford, 1996). Initial glass/melt Fe^{3+}/Fe^{2+} ratios are either high (synthetic glasses prepared in air) or low (Macusani glass; Pichavant et al., 1987) so that equilibrium Fe^{3+}/Fe^{2+} ratios were attained from either sides depending on imposed fO_2. A time series study at 200 MPa and 800°C on the Pinatubo and Ascension compositions shows that redox equilibrium conditions are attained in 15 and 3 h, respectively, and both for low and high initial Fe^{3+}/Fe^{2+} ratios (Gaillard et al., 1998).

4. Analytical techniques

After opening of the capsule, a glass fragment of about 20 mg was mounted in epoxy for electron microprobe analysis (EMPA). The remaining part of the sample was used for ferrous iron titration and infrared spectroscopy analysis.

4.1. EMPA

Glasses were analyzed for major elements with either a CAMEBAX or an SX50 electron microprobe from the BRGM-CNRS-UO Laboratories, Orléans. Operating conditions were: 15 kV acceleration voltage, 6 nA sample current, 10 s counting time on peak, beam size $10–25 \times 10–25$ μm^2 to minimize the migration of alkali (e.g., Pichavant 1987; Devine et al., 1995). A set of hydrous rhyolitic glasses, whose water contents (2.42–6.38 wt.% H_2O) were determined by pyrolysis and subsequent Karl–Fischer titration (Behrens et al., 1996), was used both to correct the concentrations of alkalis (Pichavant, 1987) and to calibrate the difference to 100% of the glass EMPA analyses (Devine et al., 1995), thus providing a first estimate of the total water content. Mineral phases present in some of the glasses were analyzed under the same operating conditions except for the beam size, which was reduced to 1–2 μm. Analytical errors are: 1% (SiO_2, Al_2O_3, CaO), 3% (FeO, MgO, TiO_2), 5% (MnO, Na_2O, K_2O).

4.2. Ferrous iron determination

The ferrous iron content of the run products was determined by colorimetric microtitration following the method of Thornber et al. (1980) and also used by Baker and Rutherford (1996). Glass chips weight-

Table 3
Effect of the quench rate on the speciation of iron and water

Starting composition	Quench rate (°C/s)	FeO[a] (wt.%)	FeO$_{tot}$[b] (wt.%)	OH/H_2O[c]
P = 200 MPa, T = 1000°C, NNO + 0.1, duration = 24 h				
Ascension	1–2	2.04 (6)	3.01 (6)	0.20 (2)
Ascension	300	2.08 (6)	2.98 (5)	0.24 (2)
No. 3	1–2	1.36 (3)	1.70 (5)	0.28 (2)
No. 3	300	1.34 (3)	1.67 (4)	0.34 (1)
P = 200 MPa, T = 800°C, NNO, duration = 24 h				
Ascension	0.5–1	1.95 (5)	2.98 (7)	0.18 (1)
Ascension	300	1.89 (5)	2.95 (6)	0.26 (1)
Pinatubo	0.5–1	0.84 (3)	1.00 (5)	0.29 (2)
Pinatubo	300	0.87 (3)	0.97 (7)	0.34 (2)
P = 200 MPa, T = 800°C, NNO − 1.6, duration = 24 h				
Ascension	0.5–1	2.49 (6)	2.98 (8)	0.15 (1)
Ascension	300	2.44 (6)	2.95 (7)	0.24 (1)

[a] Determined by volumetric titration (average of two to three analyses). Numbers in parentheses represent the analytical uncertainty (1σ level) in terms of least unit cited.

[b] Determined by electron microprobe (average of seven to eight points). Numbers in parentheses represent the analytical uncertainty (1σ level) in terms of least unit cited.

[c] Determined by infrared spectroscopy (average of three to four analyses). Numbers in parentheses represent the difference between the maximum and minimum values.

ing 50–80 mg, ground under acetone down to 10–20 μm, were used for each analysis. Glasses were first dissolved for 3 min in boiling HF and H_2SO_4, and ferrous iron in solution was titrated with $K_2Cr_2O_7$. Our method of ferrous iron titration included, with every set of unknown, the analysis of several internal standards. These included two granite international standards (Govindaraju, 1994) and a powdered sample of the June 1991 dacite from Mt. Pinatubo (FeO concentration from Bernard et al., 1991). In all cases, our results were within 1σ of the accepted values (Table 4). Other glass standards analyzed to test for the reproducibility of the ferrous iron titration method included the Pinatubo starting glass (1 wt.% FeO_{tot}, Table 1) and an alkali basalt from Etna (10 wt.% FeO_{tot}). Results of about 10 analyses carried out on each of these glasses show a maximum standard deviation (1σ) of 0.06 wt.% FeO (Table 3), slightly lower than that associated with the granitic rock powders, presumably because of the greater homogeneity of the glasses.

Several glasses were analysed in duplicate or triplicate to check for reproducibility and homogeneity of the iron redox ratio. For the 930°C charges, glasses with $FeO_{tot} < 1$ wt.% were systematically duplicated. Glasses used to establish the effect of quench rate were also systematically duplicated/triplicated, depending on the mass of sample available. When multiple analyses are available, the mean of the titrations is given (Tables 3, 5). The standard deviations on glass analyses are, as expected, dependent on the ferrous iron content. For the Pinatubo glass standard (ferrous iron = 0.34 wt.%), the stan-

dard deviation is equal to 0.02 wt.% (Table 3) and analytical uncertainties of ±0.02 wt.% have been attributed to glasses with FeO < 0.5 wt.% (Table 5). Differences between duplicate analyses for this group of samples never exceeded 0.01 wt.%, i.e., less than the attributed uncertainty. Glasses with $0.5 < \text{FeO} < 1$ wt.% have differences between duplicate analyses of ±0.03 wt.% and this value was taken as the analytical uncertainty (Tables 3, 5). For glasses with higher FeO concentrations, analytical uncertainties were calculated from standard deviations on standard glasses from Table 4, and are given on Table 3 (differences between multiple analyses always < standard deviations) and Table 5.

Fe_2O_3 (wt.%) was determined using the following equation:

$$Fe_2O_3 = (FeO_{tot} - FeO_{titration}) \times 1.1113, \qquad (5)$$

where FeO_{tot} is the total iron content, determined by EMPA (average of six to eight analyses per glass). In this study, the redox state of iron in the glass is represented by the $X_{Fe_2O_3}/X_{FeO}$ ratio, with concentrations of FeO and Fe_2O_3 in mole fractions. The error on this ratio is calculated by propagating, using standard techniques, the independent analytical uncertainties on ferrous iron (titration) and total iron (EMPA). Results are given on Table 5.

4.3. Near-infrared spectroscopy (Fourier transform infrared spectroscopy, FTIR)

Water concentration and water speciation were determined in selected glasses by FTIR. Analyses

Table 4
Reproductibility and accuracy of the ferrous iron titration method

Standard number	Number of analyses	FeO (wt.%)		
		Mean value	Standard deviation (1σ)	Accepted value
GSN[a]	30	1.68	0.08	1.65
GH[a]	15	0.94	0.06	0.91
Etna basalt[b]	10	1.78	0.06	–
Pinatubo[c]	9	0.34	0.02	–
Pinatubo dacite[d]	8	2.06	0.06	2.02

[a] International granite standard (Govindaraju, 1994).
[b] Provided by N. Métrich.
[c] Synthetic glass from Table 1.
[d] Mt. Pinatubo dacite erupted on June 15, 1991. FeO from Bernard et al. (1991).

were performed on doubly polished glass plates using a Nicolet 760 Magna FTIR spectrometer. Spectra were taken with 73 scans, resolution of 1.8 cm^{-1}, gain of 32, a CaF$_2$ beamsplitter, a visible light, and a liquid N$_2$ cooled MCT/A detector which allows to investigate in the field 11700–1200 cm^{-1}. The concentrations of OH and H$_2$O species were determined by the peak heights of the absorption bands at 4500

and 5200 cm^{-1}, respectively, using molar absorptivities from Newman et al. (1986) for rhyolitic compositions. Because of the presence of water-bearing bubbles due to water saturation, glass densities cannot be measured. Therefore, these were calculated using the model of Knoche et al. (1995) for all oxides except FeO, Fe$_2$O$_3$ (Lange and Carmichael, 1990), and H$_2$O (12 cm^3/mol; Holtz et al., 1995).

Table 5
Experimental glass compositions

NNO + 6.6

Charge number	1/1	1/2	1/3	1/4	1/7	1/8	1/9
SiO$_2$	79.11	78.41	77.91	78.05	73.23	78.33	74.51
Al$_2$O$_3$	11.86	11.90	12.08	11.97	12.69	12.68	16.21
FeO$_{total}^a$	0.54	0.80	1.15	1.18	2.95	0.91	0.62
MgO	0.00	0.00	0.00	0.00	0.01	0.23	0.03
CaO	0.00	0.00	0.00	0.00	0.36	1.36	0.23
Na$_2$O	3.83	3.95	4.10	3.89	5.71	3.39	4.45
K$_2$O	4.66	4.94	4.76	4.91	4.76	2.98	3.85
TiO$_2$	0.00	0.00	0.00	0.00	0.29	0.09	0.10
Total^b	93.06	92.89	93.34	92.76	92.66	92.62	91.38
H$_2$O (EMPA)^c	6.49	6.65	6.24	6.76	6.85	6.89	8.02
H$_2$O (infrared)^d	6.23	6.16	nd	nd	6.05	5.95	6.49
H$_2$O mol	5.07	4.95	–	–	4.98	4.85	5.24
OH mol	1.16	1.21	–	–	1.07	1.10	1.25
A/CNK	1.05	1.00	1.02	1.02	0.80	0.92	1.32
FeO^e	0.16	0.18	0.22	0.22	0.41	0.23	0.17
FeO liq^f	0.16(2)	0.18(2)	0.22(2)	0.22(2)	0.41(2)	0.23(2)	0.17(2)
Fe$_2$O$_3^g$	0.38	0.63	0.95	0.97	2.60	0.68	0.44
$X_{Fe_2O_3}/X_{FeO}^h$	1.10(26)	1.63(26)	2.01(27)	2.05(28)	2.94(18)	1.37(13)	1.21(22)

NNO + 1.55

Charge number	2/1	2/2	2/3	2/4	2/5	2/6	2/7	2/8
SiO$_2$	79.05	78.40	77.56	77.67	77.50	77.43	73.01	78.51
Al$_2$O$_3$	11.94	11.81	12.05	12.10	12.26	12.15	12.74	12.70
FeO$_{total}^a$	0.52	0.87	1.71	1.82	1.86	1.88	3.27	0.96
MgO	0.00	0.00	0.00	0.00	0.00	0.00	0.00	0.17
CaO	0.00	0.00	0.00	0.00	0.00	0.00	0.35	1.28
Na$_2$O	3.88	4.03	3.98	3.80	3.91	3.90	5.61	3.23
K$_2$O	4.61	4.89	4.70	4.62	4.47	4.64	4.77	3.01
TiO$_2$	0.00	0.00	0.00	0.00	0.00	0.00	0.26	0.09
Total^b	92.85	92.75	93.22	92.98	93.10	92.71	92.42	92.36
H$_2$O (EMPA)^c	6.71	6.81	6.36	6.59	6.48	6.85	7.12	7.18
H$_2$O (infrared)^d	nd	6.10	6.26	nd	nd	nd	6.15	nd
H$_2$O mol	–	4.97	5.11	–	–	–	1.08	–
OH mol	–	1.13	1.15	–	–	–	5.07	–
Al/(2Ca + Na + K)	1.05	0.99	1.04	1.08	1.09	1.06	0.81	0.96
FeO^e	0.38	0.60	1.11	1.39	1.69	1.95	1.72	0.76
FeO liq^f	0.38(2)	0.60(3)	1.11(4)	1.16(9)	1.19(10)	1.17(10)	1.72(5)	0.76(3)
Fe$_2$O$_3^g$	0.12	0.23	0.55	0.60	0.61	0.64	1.46	0.14
$X_{Fe_2O_3}/X_{FeO}^h$	0.14(7)	0.18(7)	0.23(5)	0.24(6)	0.24(7)	0.25(7)	0.39(3)	0.09(5)

Table 5 (*continued*)

NNO − 0.72

Charge number	3/1	3/2	3/3	3/4	3/5	3/6	3/7	3/8	3/9
SiO_2	78.97	78.41	77.50	77.20	77.37	77.09	73.60	78.88	74.86
Al_2O_3	11.96	11.88	12.08	11.71	11.67	11.61	12.55	12.42	16.26
FeO_{total}^a	0.49	0.85	1.72	2.57	2.90	3.11	3.20	0.97	0.57
MgO	0.00	0.00	0.00	0.00	0.00	0.00	0.00	0.10	0.02
CaO	0.00	0.00	0.00	0.00	0.00	0.00	0.31	1.26	0.23
Na_2O	3.91	4.07	4.11	3.92	3.78	3.66	5.42	3.38	4.24
K_2O	4.66	4.82	4.59	4.60	4.28	4.53	4.73	2.88	3.76
TiO_2	0.00	0.00	0.00	0.00	0.00	0.00	0.19	0.11	0.07
Total[b]	92,28	92,09	92,08	92,24	92,19	92,28	92,07	91,62	90,71
H_2O (EMPA)[c]	6.71	6.88	6.89	6.75	6.79	6.71	6.90	7.29	8.08
H_2O (infrared)[d]	nd	6.40	6.25	6.20	nd	nd	6.38	6.01	6.47
H_2O mol	–	5.25	5.12	5.11	–	–	5.39	4.90	5.27
OH mol	–	1.15	1.13	1.09	–	–	0.99	1.11	1.2
Al/(2Ca + Na + K)	1.04	1.00	1.03	1.02	1.07	1.06	0.83	0.94	1.37
FeO[e]	0.37	0.64	1.27	1.86	2.35	2.88	2.11	0.85	0.48
FeO liq[f]	0.37(2)	0.64(3)	1.27(4)	1.86(6)	1.87(12)	1.72(12)	2.11(6)	0.85(3)	0.48(2)
$Fe_2O_3^g$	0.10	0.17	0.37	0.60	0.93	1.32	0.97	0.06	0.04
$X_{Fe_2O_3}/X_{FeO}^h$	0.12(9)	0.12(6)	0.13(4)	0.15(3)	0.23(5)	0.34(6)	0.21(3)	0.03(4)	0.04(6)

NNO − 1.35

Charge number	4/1	4/2	4/3	4/4	4/5	4/6	4/7	4/8	4/9
SiO_2	79.02	78.66	78.14	77.80	77.75	77.39	73.63	78.78	74.70
Al_2O_3	11.95	11.99	12.18	11.90	11.83	11.83	12.81	12.84	16.50
FeO_{total}^a	0.36	0.52	0.89	1.68	2.02	2.68	2.84	0.54	0.43
MgO	0.00	0.00	0.00	0.00	0.00	0.00	0.00	0.22	0.00
CaO	0.00	0.00	0.00	0.00	0.00	0.00	0.34	1.28	0.20
Na_2O	3.92	3.90	4.03	3.97	4.02	3.65	5.47	3.39	4.35
K_2O	4.72	4.91	4.74	4.68	4.38	4.45	4.55	2.80	3.73
TiO_2	0.00	0.00	0.00	0.00	0.00	0.00	0.36	0.15	0.08
Total[b]	92,31	91,82	91,97	92,29	92,28	92,47	92,66	92,09	90,23
H_2O (EMPA)[c]	6.76	7.19	7.05	6.78	6.78	6.62	6.45	6.95	8.57
H_2O (infrared)[d]	6.39	6.25	6.21	6.25	6.14	6.10	6.10	6.21	6.63
H_2O mol	5.20	5.08	5.09	5.05	4.99	5.02	5.01	5.02	5.46
OH mol	1.19	1.17	1.12	1.20	1.15	1.08	1.09	1.19	1.17
Al/(2Ca + Na + K)	1.03	1.02	1.04	1.03	1.04	1.09	0.85	0.97	1.38
FeO[e]	0.28	0.40	0.68	1.27	1.57	2.05	1.95	0.48	0.36
FeO liq[f]	0.28(2)	0.40(2)	0.68(3)	1.27(4)	1.57(5)	2.05(6)	1.95(6)	0.48(2)	0.36(2)
$Fe_2O_3^g$	0.06	0.09	0.16	0.33	0.35	0.50	0.79	0.03	0.03
$X_{Fe_2O_3}/X_{FeO}^h$	0.10(10)	0.11(8)	0.11(6)	0.12(4)	0.10(3)	0.11(3)	0.19(3)	0.02(7)	0.04(8)

nd: not determined.

[a] Total Fe expressed as FeO.

[b] Major element oxides normalized to 100% anhydrous; original unnormalized total is reported.

[c] Estimated using the by-difference method (Devine et al., 1995).

[d] Measured by infrared spectroscopy.

[e] Ferrous iron of the bulk sample (glass + minerals) measured by wet chemistry.

[f] Ferrous iron in the glass; numbers in parentheses represent the analytical uncertainty (1σ level) in terms of least unit cited.

[g] Ferric iron in the glass calculated as $Fe_2O_3 = (FeO_{total} - FeO) \times 1.1113$.

[h] Ferric–ferrous ratio; numbers in parentheses represent the analytical uncertainty (1σ level) in terms of least unit cited.

The thickness of each sample was measured with an optical microscope equipped with an automated X–Y stage enabling measurements to within ± 1 μm.

5. Results

5.1. General

Experimental run conditions and results are given on Table 2 for 930°C and on Table 3 for 1000°C and 800°C. At these last temperatures, run products consist of glasses plus some bubbles. Only data on iron and water species concentrations are reported (Table 3) since the glasses have compositions identical to the starting products. Experimental results at 930°C are detailed on Table 5. Some of the experiments are affected by Fe loss and partial crystallization of Fe oxides and fayalite, and glass compositions may deviate from the starting compositions (Table 5).

Iron loss to the Au capsule is strongly dependent on $f\mathrm{O}_2$. The only experiment where iron loss is systematic is that performed at 930°C, NNO $-$ 1.35 (the most reduced experiment at this temperature, Table 2). The synthetic compositions are affected by Fe losses of 40% on average, and the natural by losses of 10–30% (Table 2). None of the other experiments shows significant Fe losses, including the moderately reducing run 3 (NNO $-$ 0.72, Table 2). The main practical consequence of Fe loss in run 4 (NNO $-$ 1.35) is that experimental glasses have $\mathrm{FeO_{tot}}$ contents of only half the starting compositions (Fig. 2). Formation of the Au–Fe alloy produces oxygen by reduction of FeO and $\mathrm{Fe_2O_3}$ from the melt. This oxygen is consumed by reaction with H_2 to generate a small amount of additional water at the capsule–melt interface. Overall, this does not change $f\mathrm{O}_2$ since $f\mathrm{H}_2$ is buffered and $\mathrm{H_2O}$ is in excess in all experiments. Electron microprobe traverses of charges from run 4 show homogeneous Fe concentrations in both Au capsules and glasses, suggesting that bulk equilibrium has been attained between metal and melt and, therefore, that the iron redox equilibrium (Eq. (1)) is also attained.

Run products were examined optically to check for the presence of crystals. No quench phases were detected. Crystals encountered at 930°C include haematite at NNO $+$ 6.6, magnetite at NNO $+$ 1.55 and fayalite at NNO $-$ 0.72 (Table 2). These phases appear in the most iron-rich synthetic metaluminous compositions and also in the Ascension composition at NNO $+$ 6.6. When present, they have euhedral shapes and are homogeneously distributed in the glasses. EMPA of magnetite shows that it contains minor amounts of $\mathrm{Al_2O_3}$ (less than 1.5 wt.%). Haematite crystals could not be satisfactorily analysed by electron microprobe because of their small size but were identified on the basis of their Raman spectra. Fayalite has end-member composition. The proportions of crystals present, calculated by mass balance, never exceed 3.5 wt.% (Table 2). All glasses are optically homogeneous and, when multiple analyses are available on different chips from the same glass, there is no indication for heterogeneity in $X_{\mathrm{Fe_2O_3}}/X_{\mathrm{FeO}}$.

The crystallization of Fe oxides and Fe silicates buffers the $\mathrm{FeO_{tot}}$ concentration of the melt for given T–$f\mathrm{O}_2$ conditions. Increasing the bulk $\mathrm{FeO_{tot}}$ concentration of the charges only raises the proportion of crystals present without changing the $\mathrm{FeO_{tot}}$ concentration of the melt (Table 2, Fig. 1). Saturation of metaluminous silicic melts with Fe oxides or fayalite is a strong function of $f\mathrm{O}_2$ (Fig. 1). At NNO $+$ 1, the solubility of $\mathrm{FeO_{tot}}$ in a water-saturated metaluminous silicic melt is ~ 1.7 wt.%, and it increases up to ~ 3 wt.% at FMQ. The data suggest that, at $f\mathrm{O}_2 <$ QFM, metaluminous silicic liquids can dissolve still higher amounts of iron (i.e., > 3–4 wt.% $\mathrm{FeO_{tot}}$, Fig. 1). Owing to the iron loss problem encountered at NNO $-$ 1.35, saturation of the melt with fayalite was not encountered at this $f\mathrm{O}_2$. Melt compositions from the NNO $-$ 1.35 experiment have $\mathrm{FeO_{tot}}$ contents lower than those of the NNO $-$ 0.72 experiment (Table 5, Fig. 1).

Data on the effect of quench rate on the ferric–ferrous ratio are shown on Table 3. There is no effect of quench rate on the ferric–ferrous ratio whatever the temperature and the melt composition. We thus conclude that varying the quench rate between 300°C/s and 1–3°C/s has no detectable effect on the ferric–ferrous ratio of hydrous silicic melts. In contrast, the water speciation is clearly affected (Table 3). The decoupling of the kinetics of backreaction of water species and $X_{\mathrm{Fe_2O_3}}/X_{\mathrm{FeO}}$ during quench, as observed here, does not necessarily rules out a structural interaction between water and iron in the melt (e.g., Baker and Rutherford, 1996).
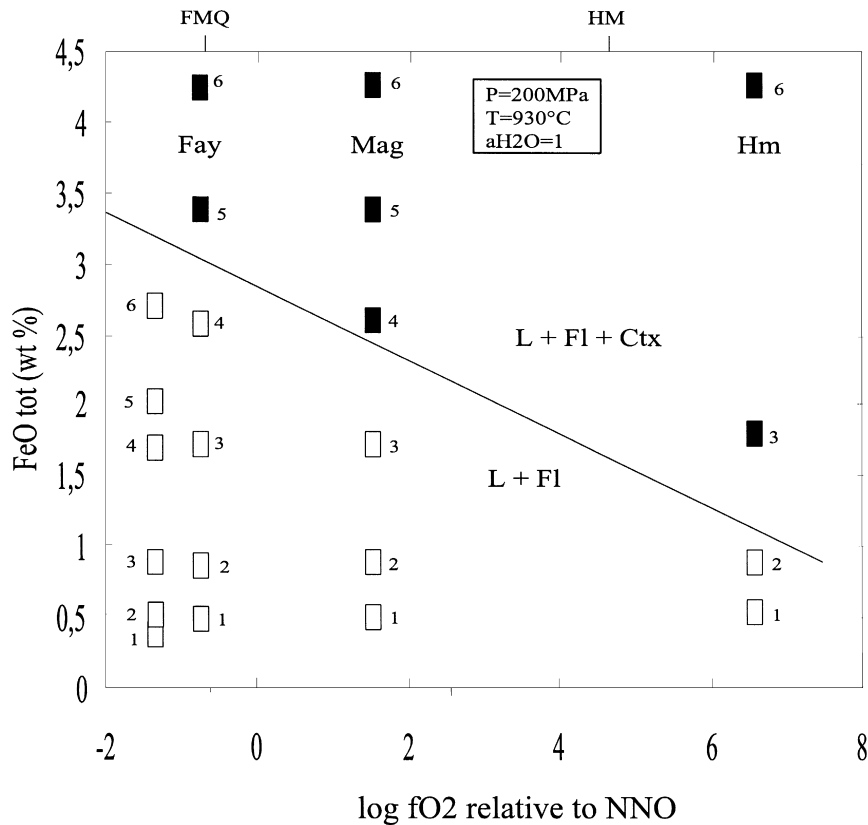
Fig. 1. Influence of fO_2 on saturation of metaluminous silicic melts with respect to Fe oxides (haematite, magnetite) or fayalite. The plotted Fe concentrations (FeO$_{tot}$) are the concentrations of the bulk charge, i.e., the concentrations of the starting glasses except for the most reducing experiment where concentrations in the experimental glasses are shown, because of Fe loss. The curve represents the solubility of FeO$_{tot}$ in the melt, constructed from experimental glass compositions in crystal-bearing charges (Table 5). Open symbols: crystal-free charges; filled symbols: crystal-bearing charges. Abbreviations: L, silicate melt; Fl, vapour phase; Ctx, crystals. The fO_2 of FMQ, and HM oxygen buffers is calculated for 930°C, 200 MPa. Number adjacent to the data points refer to the starting composition numbers (Table 1).

The lack of detectable effect of quench rate on $X_{Fe_2O_3}/X_{FeO}$ suggests that the iron redox ratio re-equilibrates either relatively slowly (in greater than a few minutes) or, alternatively, extremely rapidly (in less than a few seconds) during quench. However, oxidation–reduction cycles performed in situ at 800°C, 200 MPa under water-saturated conditions on the Pinatubo and Ascension compositions (Gaillard et al., 1998) showed that $X_{Fe_2O_3}/X_{FeO}$ re-equilibrates relatively slowly. For example, after an oxidation from NNO − 1.5 to NNO + 3 (corresponding to a fH_2 drop from 50 to ∼ 0 bar), increases of only a few percentages $X_{Fe_2O_3}/X_{FeO}$ were detected after 20 (Pinatubo) and 5 (Ascension) min, and steady-state $X_{Fe_2O_3}/X_{FeO}$ ratios were attained after

15 and 3 h, respectively. Therefore, re-equilibrating the iron redox ratio is a relatively slow process for the compositions investigated here (see also Baker and Rutherford, 1996) and the $X_{Fe_2O_3}/X_{FeO}$ ratios measured in both normally and rapidly quenched glasses reflect the redox state of iron in the melts at high P and T.

5.2. Iron redox ratio

The $X_{Fe_2O_3}/X_{FeO}$ ratio of all melt compositions at 930°C is plotted as a function of FeO$_{tot}$ for the four fO_2 values investigated (Fig. 2). For the few crystal-bearing charges, the ferric–ferrous ratio of the melt was determined from the FeO$_{tot}$ of the bulk

charge and by subtracting the contribution of the crystalline phases on the analyzed FeO content (Table 5). They have larger uncertainties due to mass balance calculations errors. The experimental $X_{Fe_2O_3}/X_{FeO}$ ratios for the series of metaluminous synthetic compositions are compared with values calculated from KC (Fig. 2). At NNO − 1.35, the

$X_{Fe_2O_3}/X_{FeO}$ ratio in the metaluminous synthetic series is constant, irrespective of the FeO_{tot} of the glass. From NNO − 0.72 and above, a positive linear dependence of this ratio with FeO_{tot} is observed, the slope of the correlation increasing with fO_2. For the most oxidizing experiment (NNO + 6.6), approximately the same amount of FeO was measured in all
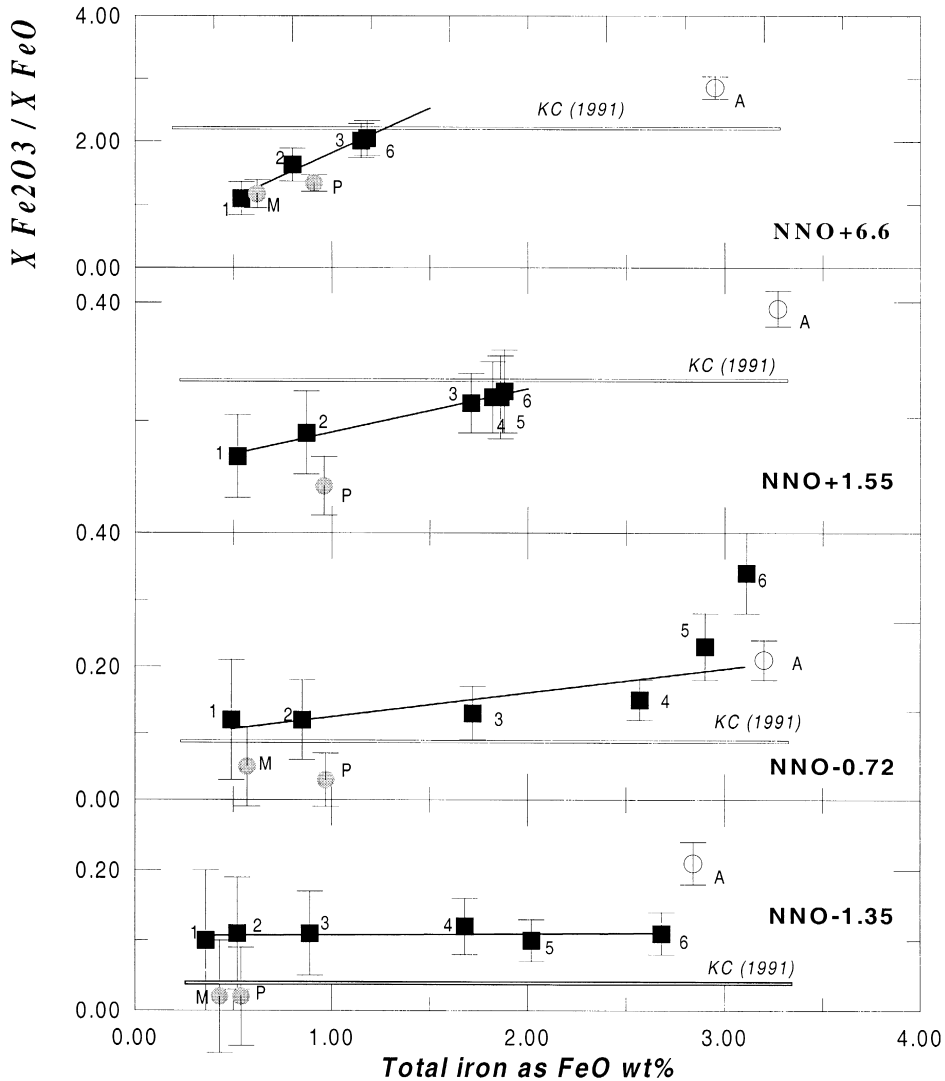
Fig. 2. The $X_{Fe_2O_3}/X_{FeO}$ ratios of hydrous silicic melts as a function of their total iron content (FeO_{tot}) for the four fO_2 values investigated at 930°C, 200 MPa. Data in Table 5. The line labelled KC shows $X_{Fe_2O_3}/X_{FeO}$ ratios calculated after Kress and Carmichael (1991) for the synthetic metaluminous compositio1ns. $X_{Fe_2O_3}/X_{FeO}$ ratios calculated after KC are weakly dependent on total iron content for the range investigated in this study and the KC line has been drawn horizontal. Solid lines are linear fits to the data points for the synthetic metaluminous glasses. Numbers adjacent to the data points refer to the starting composition number (see Table 1). M: Macusani; P: Pinatubo; A: Ascension (see Table 1).

the metaluminous synthetic compositions (Table 5). Thus, the increase of $X_{Fe_2O_3}/X_{FeO}$ with FeO_{tot} essentially results from the increase of the Fe_2O_3 species. Extrapolation of the NNO + 6.6 trend toward low total iron contents suggests that a hydrous metaluminous iron-poor ($FeO_{tot} < 0.5$ wt.%) rhyolitic melt will have a substantial fraction of iron dissolved as FeO even under these extremely oxidizing conditions. The ferric–ferrous ratios of the metaluminous synthetic compositions converge to a common value with decreasing total iron content (Fig. 2), suggesting that, at low FeO_{tot}, the ferric–ferrous ratio of hydrous metaluminous rhyolitic melts is weakly dependent on fO_2. Experimental $X_{Fe_2O_3}/X_{FeO}$ ratios determined in this study for the metaluminous compositions are either higher (NNO − 1.35, NNO − 0.72), subequal (NNO + 1.55) or lower (NNO + 6.6) than the values retrieved from the KC model. The synthetic Pinatubo composition has experimental $X_{Fe_2O_3}/X_{FeO}$ ratios in marked contrast and much lower than the other metaluminous compositions, except at the highest fO_2 (Fig. 2). For all fO_2 values, the peralkaline Ascension composition has a $X_{Fe_2O_3}/X_{FeO}$ ratio higher than the series of metaluminous compositions. In contrast, the peraluminous composition from Macusani is characterised by values of $X_{Fe_2O_3}/X_{FeO}$ lower than for the metaluminous synthetic compositions (Pinatubo excepted) and the peralkaline sample. The value for Macusani approaches those for the metaluminous compositions at the highest fO_2 (NNO + 6.6, Fig. 2).

5.3. Effect of temperature

The effect of temperature on the $X_{Fe_2O_3}/X_{FeO}$ ratio is shown on Fig. 3 for a fO_2 of NNO (Fig. 3). Data for three compositions, including the peralkaline sample from Ascension, are available in the 800–1000°C range (Tables 2, 5). No dependence of the $X_{Fe_2O_3}/X_{FeO}$ ratios with temperature is observed for the three melts studied. This conclusion agrees with the data of Baker and Rutherford (1996) at NNO + 2.5 for a peralkaline rhyolite sample compositionally similar to ours. However, the strong temperature dependence of the ferric–ferrous ratios found by Baker and Rutherford (1996) for their metaluminous composition at NNO is not confirmed
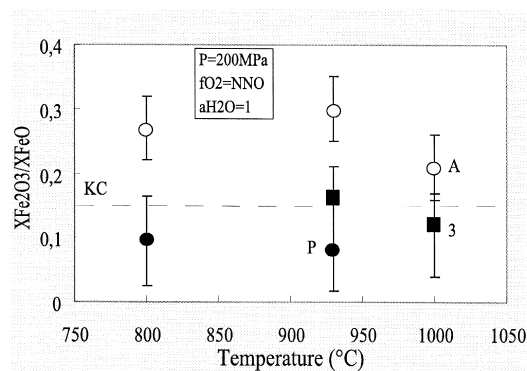

Fig. 3. Effect of temperature on the $X_{Fe_2O_3}/X_{FeO}$ ratio at NNO, 200 MPa, H_2O-saturated for the metaluminous synthetic composition no. 3 and the Ascension and Pinatubo compositions. Data in Tables 3 and 5. The 930°C $X_{Fe_2O_3}/X_{FeO}$ values are interpolated from data at this temperature for NNO − 1.15 and NNO + 1.29. The dashed line labelled KC shows $X_{Fe_2O_3}/X_{FeO}$ ratios calculated after Kress and Carmichael (1991) for the Ascension composition. Abbreviations and notations as in Fig. 2.

in the present study. Therefore, the conclusion (Kress and Carmichael, 1988; Carmichael, 1991; Carmichael and Ghiorso, 1986) — that dry silicate liquids equilibrated at different temperatures along a given oxygen buffer (e.g., NNO) have approximately constant $X_{Fe_2O_3}/X_{FeO}$ ratios — can be extended to hydrous compositions.

5.4. Water contents

The water contents estimated using the by-difference method are all similar for most glasses (average 6.5 ± 0.5 wt.%) except for the Macusani and Ascension compositions since these have high concentrations of elements not analyzed by EMPA. For metaluminous glasses, FTIR measurements suggest that the presence of iron does not largely affect the water solubility in the compositional range explored here. In particular, addition of iron up to 3 wt.% FeO_{tot} to a metaluminous rhyolite base composition produces little effect on water solubility, whatever the fO_2.

6. Discussion

6.1. Effect of water on iron speciation

If equilibrium (1) is written in terms of $FeO_{1.5}$ rather than Fe_2O_3 and assuming that both ferrous

and ferric iron mix ideally in silicate melts, we obtain the following equation (see Kress and Carmichael, 1988):

$$\log\left(X_{Fe_2O_3}/X_{FeO}\right) = 1/4\log fO_2 + \log K' + \log 2, \tag{6}$$

where

$$K' = X_{FeO_{1.5}}/\left(X_{FeO} fO_2^{1/4}\right). \tag{7}$$

Eq. (6) indicates that a linear relationship with a slope of 0.25 should be expected between $\log(X_{Fe_2O_3}/X_{FeO})$ and $\log fO_2$ if mixing of the different iron species is ideal (or if the ratio of the activity coefficients of the iron species is constant). For dry silicate melts, values of $\log(X_{Fe_2O_3}/X_{FeO})$ calculated using Eq. (3) yield a linear relation with a slope of 0.2, suggesting non-ideal mixing behaviour which has been attributed to partial clustering of ferrous and ferric iron (Kress and Carmichael, 1988; Carmichael and Ghiorso, 1990), in agreement with spectroscopic data (Virgo and Mysen, 1985).

Measured and calculated $\log(X_{Fe_2O_3}/X_{FeO})$ are plotted against $\log fO_2$ for the synthetic and natural compositions studied (Fig. 4). The relation between $\log(X_{Fe_2O_3}/X_{FeO})$ and $\log fO_2$ is nearly linear but data points $< NNO + 1$ depart from the linear trend marked by the KC line (Fig. 4). For glasses with low iron contents, data points are associated with relatively important errors (Fig. 4a,c). However, for the metaluminous glasses with $FeO_{tot} > 1$ wt.% and the Ascension composition, the relation between $\log(X_{Fe_2O_3}/X_{FeO})$ and $\log fO_2$ is not linear (Fig. 4b,c). Such a behaviour is in notable contrast with what has been observed in dry systems (Fudali, 1965; Sack et al., 1980; Kress and Carmichael, 1988; Alberto et al., 1992), where the variation of $\log(X_{Fe_2O_3}/X_{FeO})$ with fO_2 is linear for a wide range of redox conditions and melt compositions. Another important difference between hydrous and dry compositions is the strong dependence of the

ferric–ferrous ratio with FeO_{tot} for $fO_2 > NNO + 1$ (Fig. 2).

Two domains of variations of $X_{Fe_2O_3}/X_{FeO}$ with fO_2 can be distinguished. For $fO_2 < NNO + 1$, the slope of the curves (i.e., $d[\log(X_{Fe_2O_3}/X_{FeO})]/d[\log fO_2]$) progressively flattens (Fig. 4), suggesting the existence of a specific effect of water on the speciation of iron in this fO_2 range. In this region, the addition of water oxidizes iron dissolved in the melt, by reference to the expected behaviour represented by the dashed line calculated after KC (Fig. 4). In contrast, for $fO_2 > NNO + 1$, $d[\log(X_{Fe_2O_3}/X_{FeO})]/d[\log fO_2]$ approaches 0.2, i.e., is nearly equal to the slope of the dashed line calculated after KC. Therefore, in this region, the data define a relation nearly parallel to that found for dry melts. This suggests that, above $NNO + 1.5$, there is no specific effect of the presence of water on the ferric–ferrous equilibrium and ferric–ferrous ratios are essentially controlled by the anhydrous melt composition and structure for a given fO_2. It is worth emphasizing that the natural compositions (peralkaline sample from Ascension, peraluminous sample from Macusani and the metaluminous Pinatubo composition; Fig. 4c) also exhibit the same type of behaviour, with ferric–ferrous ratios distinctly flattening at low fO_2. Data points from Baker and Rutherford (1996) plotted for comparison (Fig. 4b) also illustrate the same general trend.

6.2. Predicting the iron speciation of hydrous silicic melts with the KC equation

From what precedes, it appears that water has a specific effect (i.e., oxidizing) on ferric–ferrous ratios of silicic melts from $NNO + 1.5$ and below. Under these fO_2, the KC equation predicts ferric–ferrous ratios significantly lower than the experimental values. In detail, however, there are differences between samples and it is possible to see "through"

Fig. 4. Plot of $\log(X_{Fe_2O_3}/X_{FeO})$ against $\log fO_2$ for synthetic metaluminous compositions (a: FeO_{tot} concentrations < 1 wt.%; b: FeO_{tot} concentrations > 1 wt.%) and Ascension, Macusani and Pinatubo compositions (c) at 930°C, 200 MPa, H_2O-saturated. Data in Table 5. Dashed lines labelled KC show $X_{Fe_2O_3}/X_{FeO}$ ratios calculated after Kress and Carmichael (1991) for the synthetic metaluminous compositions (a, b) and Ascension composition (c). Solid curves are polynomial fits to the data points. Data of Baker and Rutherford (1996) plotted as BR (96) with temperature indicated in degrees Celsius. Abbreviations and notations as in Fig. 2. Note the non-linear relation between experimental ferric–ferrous ratios and fO_2, and the oxidizing effect of water $< NNO + 1$ (see text).

the effect of water the influence of bulk composition on the ferric–ferrous ratio. For example, at NNO − 1.35, 930°C, $X_{Fe_2O_3}/X_{FeO}$ increases in the following order (Fig. 2): Macusani (peraluminous), series of metaluminous compositions, Ascension (peralkaline). Nevertheless, the effect of water is so important in
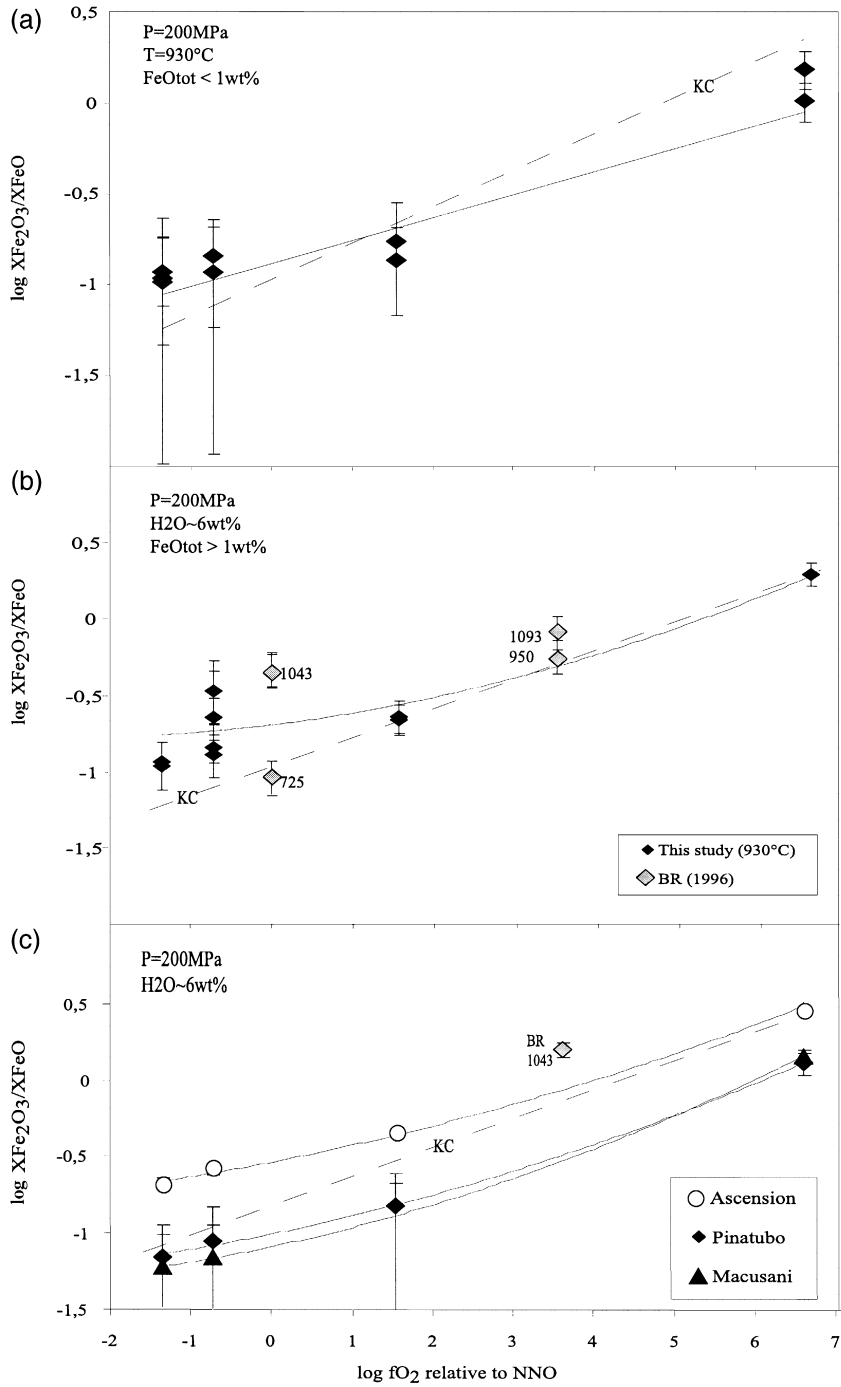
this fO_2 range that a term for dissolved water (see Baker and Rutherford, 1996) must be added to the KC equation if applied to hydrous silicic melts below NNO + 1. The correction to the KC equation is expected to be proportional to the amount of dissolved water according to Baker and Rutherford (1996). However, in H_2-buffered systems, an increase of the melt H_2O content leads to an increase of fO_2 and, therefore, the trend of increasing $X_{Fe_2O_3}/X_{FeO}$ with increasing water content observed by Baker and Rutherford (1996) can be explained by an increase of fO_2 (see also Wilke and Behrens, 1999).

Above NNO + 1.5, the ferric–ferrous ratio is essentially controlled by the anhydrous melt composition and fO_2. In this fO_2 range, it should be possible to estimate the ferric–ferrous ratios of hydrous melts by using the KC equation without an additional term describing the compositional effect of water (Moore et al., 1995). Moore et al. (1995) found no effect of dissolved water upon the speciation of iron at high fO_2 (NNO + 1–2). Baker and Rutherford (1996) showed that the presence of water has no effect on the ferric–ferrous ratio in metaluminous silicic melts at NNO + 2.5. In this study, the KC equation reproduces relatively well the experimental ferric–ferrous ratios of the hydrous metaluminous melts in the two most oxidizing runs at 930°C (Fig. 2). Yet, even in this fO_2 range, it is worth stressing that not all melt compositions have their iron redox ratio well reproduced with the KC equation. For example, experimental ferric–ferrous ratios of the peralkaline compositions studied here and by Baker and Rutherford (1996) are always higher than the calculated values, irrespective of the calculation scheme (KC or Moore et al., 1995). The reason for the discrepancy between the data of Moore et al. (1995), Baker and Rutherford (1996) and of this study for similar bulk compositions probably lies in the present limitations of the KC equation to describe subtle compositional controls on the ferric–ferrous ratio of silicic liquids. The KC equation is based on data for natural (mostly basalts and andesites) and synthetic iron-rich liquids and, as stressed by Moore et al. (1995), this compositional bias may be responsible for the KC expression being less sensitive for silicic liquids (see also Carmichael, 1991). The strong positive dependence observed be-

tween $X_{Fe_2O_3}/X_{FeO}$ and total iron content, especially at high fO_2 (Figs. 2, 4), is also not accounted for by Eq. (3). It is possible that this positive correlation is specific of silica-rich compositions. Alternatively, it may reflect the presence of water dissolved in the melt. However, a similar positive correlation between $X_{Fe_2O_3}/X_{FeO}$ and FeO_{tot} has been observed in some synthetic anhydrous systems (Mysen et al., 1980; Schreiber et al., 1980; Virgo et al., 1982; Dyar, 1985; Alberto et al., 1992). We conclude that the differences between measured and calculated ferric–ferrous ratios of silicic melts above NNO + 1 are not all attributable to the effect of dissolved water, and that additional work is needed to describe more precisely the dependence of the ferric–ferrous ratio on anhydrous melt composition.

A last characteristic of our data set that needs to be emphasized is the importance of the alkali/aluminium balance as a factor of control of the ferric–ferrous ratio of hydrous silicic liquids. The peraluminous composition (Macusani) has measured ferric–ferrous ratios persistently lower than calculated from the KC equation, even for high fO_2. In contrast, the peralkaline composition (Ascension) resides at the other end of the range, with ferric–ferrous ratios systematically higher than that calculated from KC. The series of metaluminous, Ca-free compositions occupies an intermediate position (Fig. 4b). It is worth emphasizing that at fO_2 < NNO + 1 (i.e., in the region where water has a specific oxidizing effect), the peraluminous, metaluminous and peralkaline compositions still have ferric–ferrous ratios increasing in the same order. This is consistent with a control by melt structure (alkali/aluminium balance) of the ferric–ferrous ratio. Our data under water-saturated conditions are qualitatively consistent with those of Gwinn and Hess (1989) at 1 atm and in air, suggesting that even the in presence of dissolved water, the control of the ferric–ferrous ratio by the alkali/aluminium balance remains very strong. One apparent exception to this behaviour is shown by the metaluminous Pinatubo composition, which is characterized by ferric–ferrous ratios similar to the Macusani peraluminous composition, very different from the six other metaluminous compositions (Fig. 2). We attribute this contrasted behaviour to the presence of CaO, essentially substituting for K_2O in the Pinatubo composition (Table 1). CaO and K_2O are

known to have different structural roles in alumi-nosilicate liquids, CaO being much less able than K_2O to stabilize aluminium in tetrahedral coordination. Therefore, different structural controls of the ferric–ferrous ratios are expected in CaO- and K_2O-bearing aluminosilicate melts, the former behaving more like a peraluminous melt than the latter for a given value of the alkali/aluminium balance. This provides a qualitative explanation of the different ferric–ferrous ratios observed among the different metaluminous samples and illustrates, if needed, the complexity of the compositional control of iron speciation in silicic melts.

7. Conclusions

The new experiments presented in this paper extend the iron speciation database for hydrous silicic melts toward both higher ($> NNO + 2.5$) and lower ($< NNO$) fO_2. The data, together with those from the two previous studies (Moore et al., 1995; Baker and Rutherford, 1996), form the basis of a quantitative description of the ferric–ferrous ratio of hydrous liquids as a function of temperature, dissolved melt water content, fO_2 and melt composition. The main conclusion from this study is the confirmation of a specific oxidizing effect (i.e., increase of ferric–ferrous ratio for a given fO_2) of water at $fO_2 < NNO + 1.5$ for all studied compositions (both synthetic and natural). This finding is in agreement with the previous results from Baker and Rutherford (1996). In contrast, above $NNO + 1.5$, the oxidizing effect of water is lost and iron speciation is controlled by anhydrous melt composition and structure, besides fO_2, as reported previously by Moore et al. (1995). It follows that a term for dissolved water must be added to the empirical equations describing the compositional dependence of the iron redox ratio, if to be applied to the calculation of ferric–ferrous ratios of hydrous silicic melts below $NNO + 1.5$. Another implication from this study is that the iron species in the melt cannot be considered to mix ideally and that their activity coefficients depend on fO_2 and also FeO_{tot}. Significant differences exist between measured and calculated ferric–ferrous ratios of silicic melts that are not all attributable to the effect of dissolved water, so that additional work is needed to describe more accurately the dependence of the ferric–ferrous ratio on anhydrous melt composition.

It is worth emphasizing here that the oxidizing effect of water demonstrated in this study is restricted to moderately to fairly reduced magmatic liquids. So far, ferric–ferrous ratios of hydrous liquids have not been examined systematically below $NNO − 1.5$, which is not so reduced a fO_2 considering the range of redox conditions for natural magmas (e.g., Carmichael, 1991). Therefore, for hydrous calk-alkaline magmatic liquids that have fO_2 in the range $NNO + 1$ to $NNO + 3$, no specific effect of the presence of dissolved water on ferric–ferrous ratios is expected. It follows that the oxidizing nature of these magmas is not due to the presence of (sometimes) large amounts of dissolved water, but reflects either the intrinsically oxidized nature of the calk-alkaline magma series or loss of H_2 during magmatic evolution.

Acknowledgements

References

Alberto, H.V., Gil, J.M., Ayres DeCampos, N., Mysen, B.O., 1992. Redox equilibria of iron in Ti-bearing calcium silicate-quenched glasses. J. Non-Cryst. Sol. 151, 39–50.

Baker, L., Rutherford, M.J., 1996. The effect of dissolved water on the oxidation state of silicic melts. Geochim. Cosmochim. Acta 60, 2179–2187.

Behrens, H., Romano, C., Nowak, M., Holtz, F., Dingwell, D.B., 1996. Near-infrared spectroscopic determination of water species in glasses of system $MAlSi_3O_8$ (M = Li, Na, K): an interlaboratory study. Chem. Geol. 128, 41–63.

Borisov, A.A., Shapkin, A.I., 1990. A new empirical equation relating Fe^{3+}/Fe^{2+} in magmas to their composition, oxygen fugacity, and temperature. Geokhimiya 6, 892–897.

Burnham, C.W., Holloway, J.R., Davis, N.F., 1969. Thermodynamic properties of water to 1000°C and 10,000 bar. Geol. Soc. Am., Spec. Pap. 132, 1–96.

Bernard, A., Demaiffe, D., Mattielli, N., Punongbayan, R.S., 1991. Anhydrite-bearing pumices from Mount Pinatubo: further evidence for the existence of sulfur-rich silicic magmas. Nature 743, 210–415.

Carmichael, I.S.E., 1991. The redox state states of basic and silicic magmas: a reflection of their source regions? Contrib. Mineral. Petrol. 106, 129–141.

Carmichael, I.S.E., Ghiorso, M.S., 1986. Oxidation–reduction relations in basic magmas: a case for homogeneous equilibria. Earth Planet. Sci. Lett. 78, 200–210.

Carmichael, I.S.E., Ghiorso, M.S., 1990. The effect of oxygen fugacity on the redox state of natural liquids and their crystallising phases. In: Nicholls, J., Russell, J.K. (Eds.), Understanding Magmatic Processes. Modern Methods of Igneous Petrology. Rev. Mineral., vol. 24, pp. 191–212.

Devine, J.D., Gardner, J.E., Brach, H.P., Layne, G.D., Rutherford, M.J., 1995. Comparison of microanalytical methods for estimation of H_2O content of silicic volcanic glasses. Am. Mineral. 80, 319–328.

Dickenson, M.P., Hess, P.C., 1981. Redox equilibria and the structural role of iron in aluminosilicate melts. Contrib. Mineral. Petrol. 78, 352–357.

Dickenson, M.P., Hess, P.C., 1986. The structural role and homogeneous redox equilibria of iron in peraluminous: metaluminous and peralkaline silicate melts. Contrib. Mineral. Petrol. 92, 207–217.

Dingwell, D.B., 1991. Redox viscosimetry of some iron-bearing silicate liquids. Am. Mineral. 76, 1560–1562.

Dingwell, D.B., Brearley, M., 1988. Melt density in the CaO–FeO–Fe_2O_3–SiO_2 system and the compositional dependence of the partial molar volume of ferric iron in silicate melts. Geochim. Cosmochim. Acta 52, 2815–2825.

Douglas, R.W., Nath, P., Paul, A., 1965. Oxygen ion activity and its influence on the redox equilibrium in glasses. Phys. Chem. Glasses 6, 216–225.

Dyar, M.D., 1985. A review of Mössbauer data on inorganic glasses: the effect of composition on iron valency and coordination. Am. Mineral. 70, 304–316.

Fudali, R.F., 1965. Oxygen fugacities of basaltic and andesitic magmas. Geochim. Cosmochim. Acta 29, 1063–1075.

Gaillard, F., Scaillet, B., Pichavant, M., 1998. Kinetics of iron oxidation–reduction in hydrous silicic melts. Terra Nova 10, 17.

Govindaraju, K., 1994. Compilation of working values and sample description for 383 geostandards. Geostand. Newsl. 18, 158 pp.

Gwinn, R., Hess, P.C., 1989. Iron and titanium properties in peraluminous and peralkaline rhyolitic liquids. Contrib. Mineral. Petrol. 101, 326–338.

Harris, C., 1983. The petrology of lavas and associated plutonic inclusions of Ascension Island. J. Petrol. 24, 424–470.

Holloway, J.R., Dixon, J.E., Pawley, A.R., 1992. An internally heated, rapid-quench, high-pressure vessel. Am. Mineral. 77, 643–646.

Holtz, F., Pichavant, M., Barbey, P., Johannes, W., 1992. Effects of H_2O on liquidus phase relations in the haplogranite system at 2 and 5 kbar. Am. Mineral. 77, 1223–1241.

Holtz, F., Behrens, H., Dingwell, D., Johannes, W., 1995. H_2O solubility in haplogranitic melts: compositional, pressure, and temperature dependence. Am. Mineral. 80, 94–108.

Johnson, M.C., Anderson, A.T., Rutherford, M.J., 1994. Pre-eruptive volatile contents of magmas. In: Carroll, M., Holloway, J. (Eds.), Volatiles in Magmas. Rev. Mineral., vol. 30, pp. 281–323.

Kilinc, A., Carmichael, I.S.E., Rivers, M.L., Sack, R.O., 1983. The ferric ratio of natural silicate liquids equilibrated in air. Contrib. Mineral. Petrol. 83, 136–140.

Knoche, R., Dingwell, D.B., Weeb, S.L., 1995. Leucogranitic and pegmatitic melt densities: partial molar volumes for SiO_2, Al_2O_3, Na_2O, Rb_2O, Cs_2O, Li_2O, BaO, SrO, CaO, MgO, TiO_2, B_2O_3, P_2O_5, F_2O_1, Ta_2O_5, Nb_2O_5 and WO_3. Geochim. Cosmochim. Acta 50, 435–443.

Kress, V.C., Carmichael, I.S.E., 1988. Stoichiometry of the iron oxidation reaction in silicate melts. Am. Mineral. 73, 1267–1274.

Kress, V.C., Carmichael, I.S.E., 1991. The compressibility of silicate liquids containing Fe_2O_3 and the effect of composition: temperature: oxygen fugacity and pressure on their redox states. Contrib. Mineral. Petrol. 108, 82–92.

Lange, R., Carmichael, I.S.E., 1990. Thermodynamic properties of silicate liquids with emphasis on density, thermal expansion and compressibility. In: Nicholls, J., Russell, J.K. (Eds.), Understanding Magmatic Processes. Modern Methods of Igneous Petrology. Rev. Mineral., vol. 24, pp. 25–64.

Martel, C., Pichavant, M., Bourdier, J.L., Traineau, H., Holtz, F., Scaillet, B., 1998. Magma storage conditions and control of eruption regime in silicic volcanoes: experimental evidence from Mt. Pelée. Earth Planet. Sci. Lett. 156, 815–823.

Moore, G., Righter, K., Carmichael, I.S.E., 1995. The effect of dissolved water on the oxidation state of iron in natural silicate liquids. Contrib. Mineral. Petrol. 120, 170–179.

Mysen, B.O., 1988. Structure and Properties of Silicate Melts. Elsevier, Amsterdam.

Mysen, B.O., Seifert, F.A., Virgo, D., 1980. Structure and redox equilibria of iron-bearing silicate melts. Am. Mineral. 65, 867–884.

Newman, S., Stolper, E.M., Epstein, S., 1986. Measurement of water in rhyolitic glasses: calibration of an infrared spectroscopic technique. Am. Mineral. 71, 1521–1527.

Osborn, E.F., 1959. Role of oxygen pressure in the crystallisation and differentiation of basaltic magma. Am. J. Sci. 257, 609–647.

Pichavant, M., 1987. Effects of B and H_2O on liquidus phase relations in the haplogranite system at 1 kbar. Am. Mineral. 72, 1056–1070.

Pichavant, M., Herrera, J.V., Boulmier, S., Briqueu, L., Joron, J.-L., Juteau, M., Marin, L., Michard, A., Sheppard, S.M.F., Treuil, M., Vernet, M., 1987. The Macusani glasses, SE Peru: evidence of chemical fractionation in peraluminous magmas. In: Mysen, B.O. (Ed.), Magmatic Processes: Physicochemical Principles. The Geochemical Society, pp. 359–373, Special Publication No. 1.

Pownceby, M.I., O'Neill, H.St.C., 1994. Thermodynamic data from redox reactions at high temperatures: III. Activity composition relations in Ni–Pd alloys from EMF measurements at 850–1250 K, and calibration of the NiO + Ni–Pd assemblage as a redox sensor. Contrib. Mineral. Petrol. 116, 327–339.

Robie, R.A., Hemingway, B.S., Fisher, J.R., 1978. Thermody-

namic properties of minerals and related substances at 298.15 K and 1 bar (10^5 Pascals) pressure and at higher temperature. Geol. Surv. Bull. 1452, 456.

Roux, J., Lefèvre, A., 1992. A fast-quench device for internally heated pressure vessels. Eur. J. Mineral. 4, 279–281.

Sack, R.O., Carmichael, I.S.E., Rivers, M., Ghiorso, M.S., 1980. Ferric–ferrous equilibria in natural silicate liquids at 1 bar. Contrib. Mineral. Petrol. 75, 369–376.

Scaillet, B., Evans, B.W., 1999. The June 15, 1991 eruption of Mount Pinatubo: I. Phase equilibria and pre-eruption $P-T-fO_2-fH_2O$ conditions of the dacite magma. J. Petrol. 40, 381–411.

Scaillet, B., Pichavant, M., Roux, J., Humbert, G., Lefèvre, A., 1992. Improvements of the Shaw membrane technique for measurement and control of fH_2 at high temperatures and pressures. Am. Mineral. 77, 647–655.

Scaillet, B., Pichavant, M., Roux, J., 1995. Experimental crystallisation of leucogranite magmas. J. Petrol. 36, 663–705.

Schreiber, H.B., Lauer, H.V., Thanyasiri, T., 1980. Oxidation–reduction equilibria of iron and cerium in silicate glasses: individual redox potentials and mutual interactions. J. Non-Cryst. Solids 38–39, 785–790.

Taylor, J.R., Wall, V.J., Pownceby, M.I., 1992. The calibration and application of accurate redox sensor. Am. Mineral. 77, 284–295.

Thornber, C.R., Roedder, P.L., Foster, J.R., 1980. The effect of composition on the ferric–ferrous ratio in basaltic liquids at atmospheric pressure. Geochim. Cosmochim. Acta 44, 525–532.

Virgo, D., Mysen, B.O., 1985. The structural state of iron in oxidised vs. reduced glasses at 1 atm: a 57 Fe Mössbauer study. Phys. Chem. Miner. 12, 65–76.

Virgo, D., Mysen, B.O., Danckwerth, P., Seifert, F., 1982. Speciation of Fe^{3+} in 1 atm Na_2O-SiO_2-Fe-O melts. Carnegie Inst. Washington, Year Book 81, 349–353.

Wilke, M., Behrens, H., 1999. The dependence of the partitioning of iron and europium between plagioclase and hydrous tonalitic melt on oxygen fugacity. Contrib. Mineral. Petrol. 137, 102–114.